analytical chemistry

pubs.acs.org/ac Article

Photoactivated DNA Walker Based on DNA Nanoflares for Signal-Amplified MicroRNA Imaging in Single Living Cells

Mengxi Chen, Ruilin Duan, Shijun Xu, Zhijuan Duan, Quan Yuan, Fan Xia, and Fujian Huang*

Cite This: https://doi.org/10.1021/acs.analchem.1c04505 Read Online

ACCESS | Metrics & More | Article Recommendations | Supporting Information

ABSTRACT: Specific and sensitive detection and imaging of cancer-related miRNA in living cells are desirable for cancer diagnosis and treatment. Because of the spatiotemporal variability of miRNA expression level during different cell cycles, signal amplification strategies that can be activated by external stimuli are required to image miRNAs on demand at desired times and selected locations. Herein, we develop a signal amplification strategy termed as the photoactivated DNA walker based on DNA nanoflares, which enables photocontrollable signal amplification imaging of cancer-related miRNA in single living cells. The developed method is achieved *via* combining photoactivated nucleic acid displacement reaction with the traditional exonuclease III (EXO III)-assisted DNA walker based on DNA nanoflares. This method is capable of on-demand activation of the DNA walker for dictated signal amplification imaging of cancer-related miRNA in single living cells. The developed method was demonstrated as a proof of concept to achieve photoactivated signal amplification imaging of miRNA-21 in single living HeLa cells *via* selective two-photon irradiation (λ = 740 nm) of single living HeLa cells by using confocal microscopy equipped with a femtosecond laser.

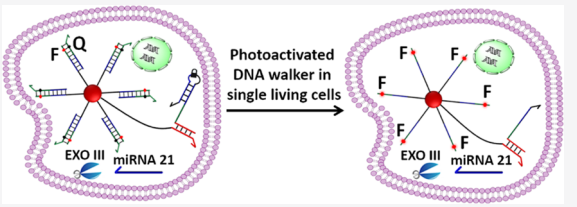

INTRODUCTION

In recent years, due to the small size and low abundance of miRNAs in cells,[1] specific and sensitive imaging of cancer-related miRNA has been promising because of the important applications in risk prediction,[2] drug discovery,[3] diagnosis,[4] and disease treatment.[5] Strategies capable of signal amplification are promising to achieve sensitive detection and imaging of target miRNA.[6−12] One of the signal amplification methods is to reuse the target miRNA to continuously release signals.[13] Exonuclease III (EXO III) could assist cascade signal amplification by regenerating and recycling the target nucleic acid.[14] EXO III-assisted nucleic acid signal amplification is wildly used for signal amplification biosensors and bioimaging.[15−20]

For signal amplification during detection, a DNA walker which could constantly move along a designed DNA track has also been used to achieve sensitive target nucleic acid detection.[6,21−24] Particularly, a DNA walker based on DNA nanoflares[25−27] is widely used for signal amplification imaging of target miRNA in living cells.[28−31] Enzymes such as EXO III or DNAzyme are generally used as an energy source that complements and enhances the strand displacement strategy to enhance the efficiency of DNA walker motion.[22,32,33] DNAzyme has sequence dependence, which sometimes limits its applications. EXO III, in contrast, is more versatile.

Signal amplification miRNA detection in biological systems has been researched in previous research works.[34−37] Since the expression level and subcellular distribution of miRNAs vary dynamically during different cell cycles,[38] signal amplification methods that can be activated by external stimuli are required to achieve on-demand imaging of miRNAs at desired time points and selected locations. However, the present EXO III-assisted DNA walker based on DNA nanoflares for signal amplification detection and imaging is difficult to precisely control the localization at desired time points, and it remains a challenge to precisely trigger the DNA walker on the DNA nanoflare surface at desired times and positions to achieve dictated target detection and imaging in living cancer cells.

Light is an effective trigger for the precise spatiotemporal activation of photoresponsive functional DNA. With the introduction of a photocleavable linker (PC-linker) into the DNA strand, precise spatiotemporal activation of functional DNA could be realized by controllable irradiation.[39] Our group has applied this photoresponsive functional DNA for DNA photolithography and patterning,[40−43] electrochemical biosensing,[44] drug delivery,[45,46] and photoactivated biosensing in single living cells.[19,47,48]

Inspired by the above arguments, we propose here a new strategy named photoactivated DNA walker based on DNA nanoflares for dictated signal amplification miRNA-21 imaging in single living cells. The developed strategy combines the previously developed photoactivated nucleic acid displacement

Received: October 18, 2021
Accepted: November 10, 2021

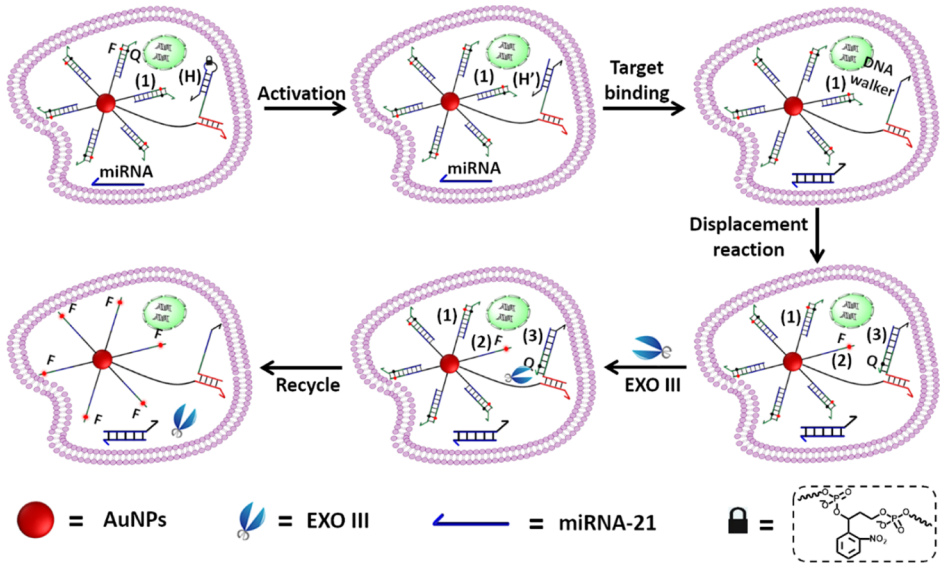

Figure 1. Schematic overview of UV light-photoactivated DNA walker based on DNA nanoflares in HeLa cells for dictated signal amplification miRNA imaging. The DNA hairpin on the AuNPs was activated via UV irradiation. The activated DNA hairpin triggered the displacement reaction with target miRNA and the subsequent DNA walker signal amplification process with the assistance of EXO III.

reaction and the Exo III-assisted DNA walker based on DNA nanoflares for controlled nucleic acid cascade recycling amplification. The designed photocontrollable DNA walker based on DNA nanoflares is capable of on-demand activation of the biosensing process in living cells. We demonstrated this process by using it to achieve photoactivated signal-amplified imaging of miRNA in single living cancer cells.

EXPERIMENTAL SECTION

Chemicals and Reagents. Tris(2-carboxyethyl) phosphine hydrochloride (TCEP), chloroauric acid ($HAuCl_4 \cdot 4H_2O$), and 6-hydroxy-1-hexanethiol (MCH) were obtained from Sigma-Aldrich. Phosphate-buffered saline (PBS, 0.1 M) buffer and 10 × TBE were purchased from Sangon Biotechnology Co., Ltd. (Shanghai, China). Fetal bovine serum and Dulbecco's modified Eagle's medium (DMEM) were purchased from Gibco. The HeLa cell was obtained from the cell bank of the committee on type culture collection of the Chinese Academy of Sciences (Shanghai, China). Other chemicals were obtained from Sinopharm Chemical Reagents Co., Ltd. (Shanghai, China) and used without further purification. All solutions were dissolved with Milli-Q water from a Millipore system. Oligonucleotides were purchased from Hippo Biotechnology Co., Ltd. (Beijing, China), and the detailed sequences are shown in Supporting Information, Table S1.

Instruments. A UV lamp (LUYOR-365, China) was used to activate the DNA walker at a power density of 7 mW/cm^2. A Shimadzu UV-2600 spectrophotometer (Shimadzu, Japan) was used to record the UV−vis absorption spectra. A FS5 fluorescence spectrophotometer was used to measure fluorescence spectra using excitation at 542 nm. Confocal microscopy images were obtained using a Zeiss LSM 880 confocal microscope. The scanning electron microscopy (SEM) images were obtained on a SU-8010 field emission scanning electron microscope (Hitachi, Japan).

Preparation of DNA Nanoflares. The AuNPs were first prepared by a classic sodium citrate reduction method. Briefly, 100 mL of 0.006 wt % $HAuCl_4$ was heated to boil for 5 min on a hot plate with vigorous stirring. Then, 3 mL of 1 wt % sodium citrate solution was rapidly added after boiling. Boiling was continued for another 30 min until the solution changed into wine red. The reaction was terminated by removing the heating source and cooling slowly to room temperature. The prepared AuNP solution was stored at 4 °C for further use. SEM images indicated that the particle size was 13 ± 2 nm. The concentration of AuNPs was determined by measuring their absorbance at 520 nm ($\varepsilon = 5.502 \times 10^8$ L mol^{-1} cm^{-1}).

After reduced by TCEP, thiolated DNA (**F**) and (**L**) (detailed sequences are shown in Supporting Information, Table S1) were mixed with AuNPs at a mole ratio of 400:20:1 for 16 h with shaking at 4 °C. Then, sodium phosphate buffer (PBS, 5 M of NaCl, 200 mM of Na_2HPO_4 and NaH_2PO_4, pH = 7.4) was added to the mixture (a total of five salting steps with 2 h intervals between steps) to reach a final concentration of 0.3 M of NaCl and 10 mM of Na_2HPO_4 and NaH_2PO_4. This salting process was incubated for another 40 h under shaking. After that, the DNA nanoflares were prepared and washed with 0.1 M PBS three times to remove excess DNA through centrifugation. Then, the DNA nanoflares were resuspended in 0.1 M PBS. After that, excess DNA (**Q**) and (**H**) were added into DNA nanoflares and incubated for 1 h to hybridize with DNA (**F**) and (**L**) modified on the AuNP surface. The incubated DNA nanoflares were then washed with 0.1 M PBS two times and resuspended in 0.1 M PBS.

Fluorescence Measurements. Fluorescence intensity was measured under different conditions using excitation at 542 nm. Photoactivated toehold-mediated displacement reaction in the buffer solution was followed by measuring the fluorescence intensity in a 60 μL solution consisting of 300 nM double-strand DNA (**1**) and 100 nM (**H**) probe complex detection for 0, 20, 40, 60, 80, and 100 nM target miRNA (with or without UV irradiation). The photoactivated signal amplification was performed in a 60 μL solution consisting of 300 nM (**F**) + (**Q**) probe complex and 100 nM (**H**) probe or DNA nanoflares. The mixture solutions were irradiated with UV light for 3 min; then, target miRNA-21 or the target with base mutations and 0.5 U/μL EXO III were added into the solution, and the

https://doi.org/10.1021/acs.analchem.1c04505
Anal. Chem. XXXX, XXX, XXX−XXX

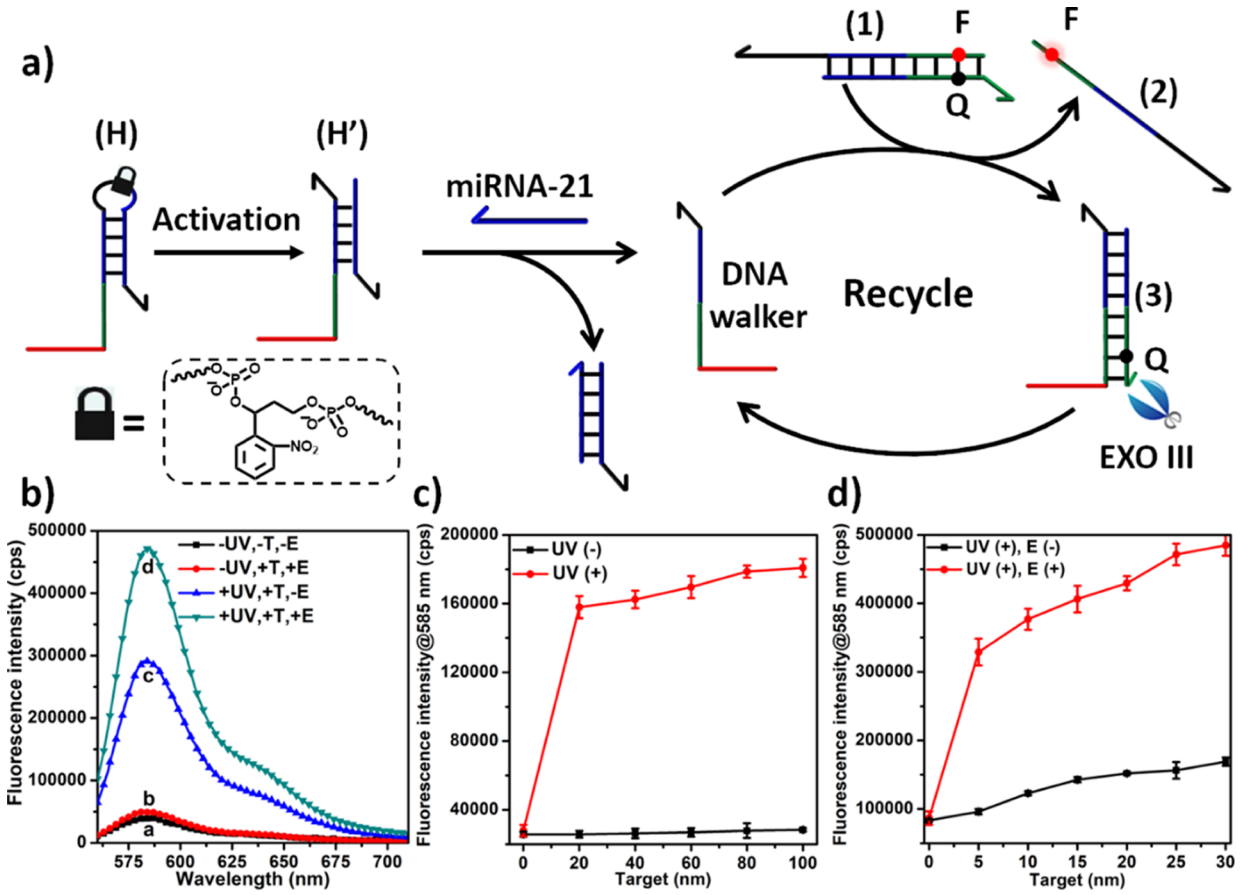

Figure 2. Photoactivated DNA walker signal amplification process in solution. (a) Schematic of the photocontrollable signal amplification. (b) Fluorescence spectra of the (**1**) and (**H**) mixture solution under different conditions. (c) Fluorescence intensity of the mixture solutions without and with UV irradiation in the presence of miRNA-21 with different concentrations. The concentration of photoresponsive DNA hairpin (**H**) is 100 nM, and the concentration of double-strand DNA (**1**) is 300 nM. (d) Fluorescence intensity of the UV-irradiated mixture solutions without and with EXO III treatment in the presence of miRNA-21 with different concentrations. The concentration of photoresponsive DNA hairpin (**H**) is 100 nM, the concentration of double-strand DNA (**1**) is 300 nM, and the concentration of EXO III is 0.5 U/μL. Error bars derived from $N = 3$ experiments.

fluorescence intensity was measured after 90 min incubation at 37 °C under light shielding.

Cell Culture. HeLa cells were grown in DMEM with 10% fetal bovine serum and 1% penicillin−streptomycin at 37 °C in a humid atmosphere with 5% CO_2.

Incubation of HeLa Cells with DNA Nanoflares. Cells was seeded on a cell culture dish and further incubated to grow to about 80% confluence. The cultured cells were washed using 1 × PBS three times. Then, 400 μL of Opti-MEM containing 0.67 nM DNA nanoflares was added into the washed cells. The cells were further cultured for 4 h at 37 °C with 5% CO_2. For EXO III transfection, 400 μL of Opti-MEM containing lipofectamine 2000 (1 mg/mL, 1 μL) and EXO III (2 U/μL, 10 μL) was added into the cells and incubated at 37 °C for 1 h.

Laser Scanning Confocal Microscopy Imaging. After incubation, the excess DNA nanoflares were removed *via* cell washing three times with 1 × PBS. Cells were then irradiated for 5 min with UV light. The cells were imaged with a 63× oil immersion objective on a laser scanning confocal microscope (Zeiss LSM 880). For the photoactivation of DNA nanoflares in single living cells, the cells were selectively irradiated by using a laser scanning confocal microscope with a femtosecond laser at λ = 740 nm.

Cytotoxicity Tests. The cytotoxicity of DNA nanoflares, EXO III, and UV irradiation on HeLa cells was evaluated using MTT assays. First, HeLa cells (5×10^3 cells/mL) were seeded on 96-well plates and grown for 24 h. The cells were treated with 0.67 nM DNA nanoflares and 2 U/μL EXO III for 24 h and irradiated with UV light for 10 min (7 mW cm^{-2}). After irradiation, the cells were further incubated for different time periods. After that, 20 μL of the MTT test solution (5 mg/mL) was added into the treated cells to further incubate for 4 h at 37 °C. After 4 h incubation, the supernatant was removed and DMSO (150 μL) was added to the cells. A microplate reader was used to measure the absorbance values at 570 nm.

RESULTS AND DISCUSSION

Principle of the Photoactivated DNA Walker Based on DNA Nanoflares for Signal-Amplified miRNA Imaging in Living Cells. Figure 1 schematically shows the whole process of the photoactivatable DNA walker based on DNA nanoflares for signal amplification miRNA imaging in living cancer cells. Photoactivatable hairpin DNA (**H**) containing the DNA walker and DNA duplex track (**1**) consisting of TAMRA-modified single strands and fluorophore quencher-modified single strands were immobilized on the AuNP surface. These fabricated DNA nanoflares can be easily

https://doi.org/10.1021/acs.analchem.1c04505
Anal. Chem. XXXX, XXX, XXX−XXX

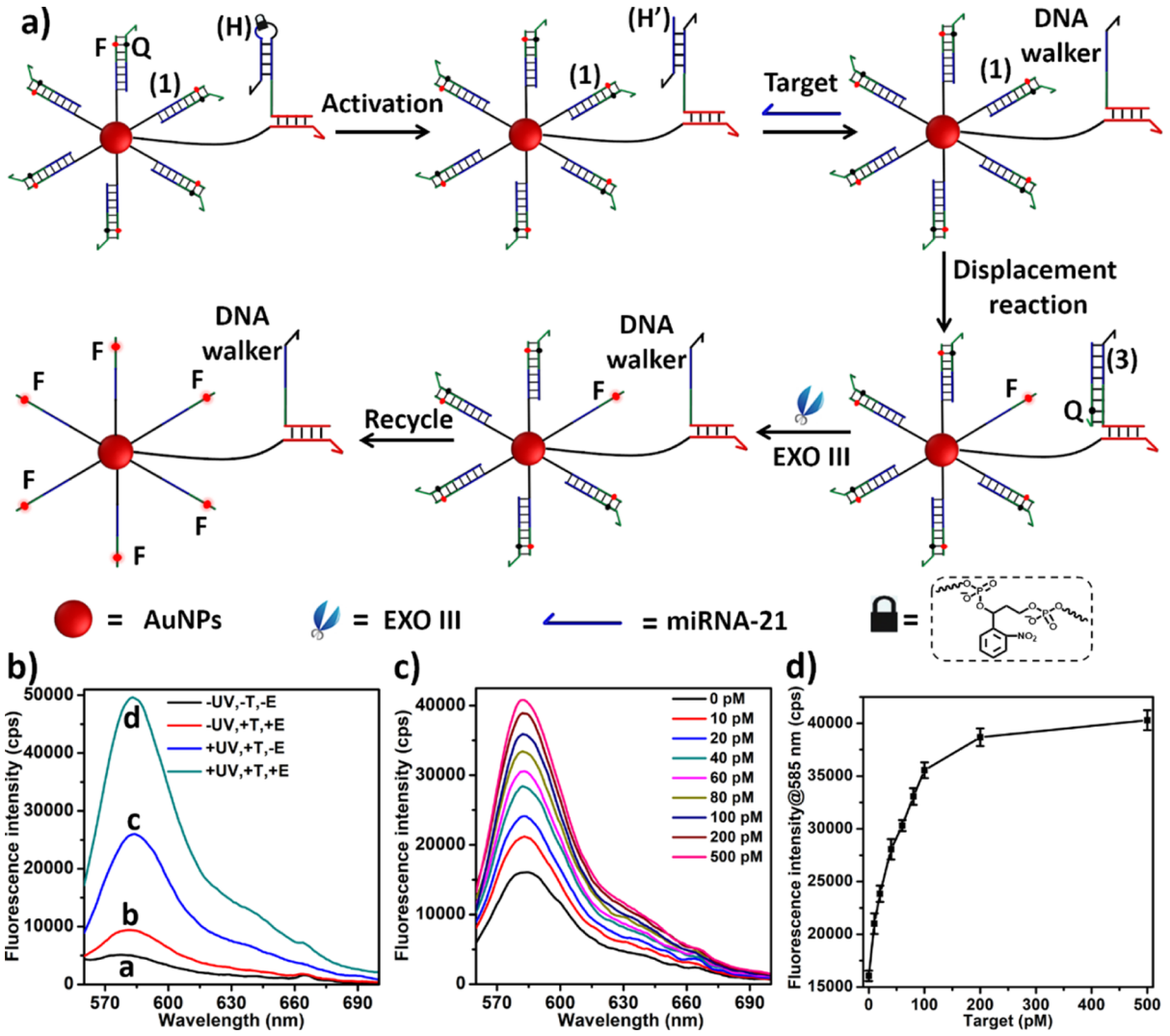

Figure 3. Light-activated DNA walker cascade recycling amplification reaction based on DNA nanoflares in solution. (a) Principle of the photoactivated DNA walker signal amplification process on the DNA nanoflare surface. (b) Fluorescence spectra of the photocontrollable DNA nanoflares under different conditions. (c) Fluorescence intensity of the UV-irradiated DNA walker system under different miRNA-21 concentrations with EXO III treatment. (d) Plot of fluorescence intensity of the system at 585 nm vs target concentration (Error bars derived from $N = 3$ experiments). The concentration of the DNA nanoflares used in these experiments was 1.44 nM.

endocytosed into living cancer cells. Light was used to activate the photoresponsive hairpin DNA on the DNA nanoflares to trigger the displacement reaction with target miRNA-21, releasing the DNA walker strand in activated hairpin DNA. The released DNA walker then hybridized with the fluorophore quencher-modified DNA strand in the DNA duplex track *via* the toehold-mediated displacement reaction to release the TAMRA-modified DNA strand on the AuNP surface with turn-on fluorescence. The fluorophore quencher-modified DNA strand hybridized with the DNA walker could then be hydrolyzed from its recessed 3-termini to regenerate the DNA walker circularly. Thus, the signal amplification miRNA imaging in living cells *via* the DNA walker on the DNA nanoflare surface was successfully controlled *via* UV irradiation.

Photoactivated DNA Walker System in Solution. First, the photoactivated DNA walker system in solution was characterized and evaluated using fluorescence spectra. Figure 2a shows the whole process of the light-activated DNA walker system in solution. As can be seen, the photoresponsive DNA hairpin (**H**) with 3′-protruding termini was activated by UV irradiation to form the activated double-strand DNA structure (**H′**) with 3′-protruding termini and the activated toehold. The DNA walker strand was then released from the activated (**H′**) *via* toehold-mediated displacement reaction in the presence of target miRNA. The released DNA walker strand then hybridized with the fluorophore quencher-labeled DNA strand in double-strand DNA (**1**) through the toehold-mediated displacement reaction, releasing TAMRA-modified single-strand DNA and forming double-strand DNA (**3**) with recessed 3′-termini. EXO III prefers to hydrolyze the substrates with recessed or blunt 3′-termini, while 3′-protruding termini are resistant to hydrolysis. Thus, the fluorophore quencher-labeled single strand in newly formed double-strand DNA (**3**) was hydrolyzed from 3′-protruding termini to regenerate the DNA walker, and the regenerated DNA walker could trigger new cycles to continuously release the fluorescence signal.

To confirm that the whole process was indeed processed as described in Figure 2a, the fluorescence of the photoactivatable DNA hairpin (**H**) and double-strand track DNA (**1**) mixture

https://doi.org/10.1021/acs.analchem.1c04505
Anal. Chem. XXXX, XXX, XXX−XXX

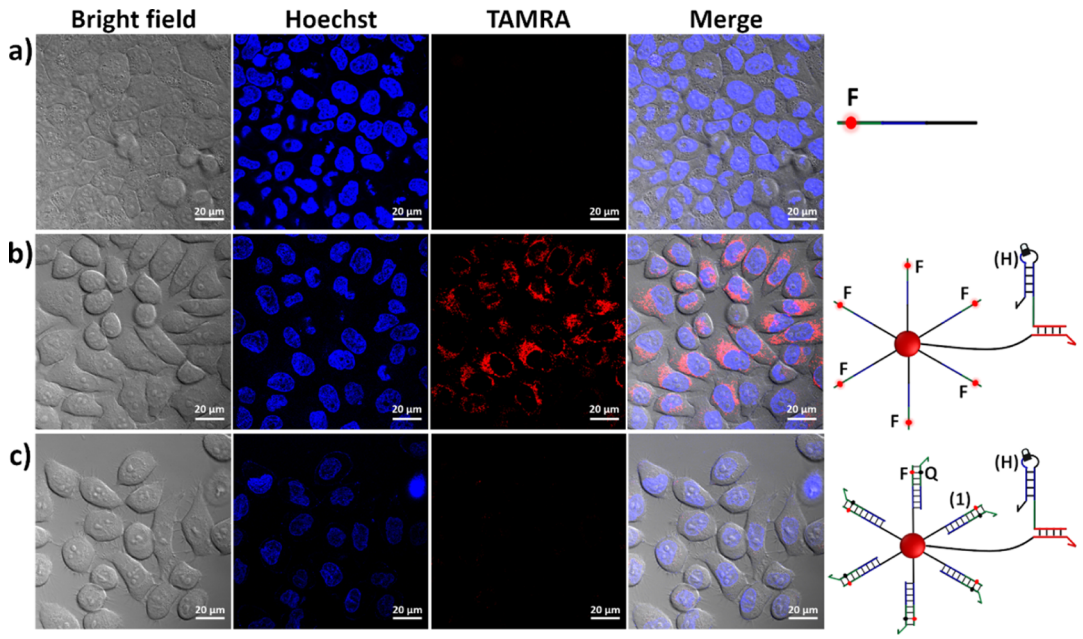

Figure 4. Laser scanning confocal microscopy imaging of HeLa cells treated with different probes. (a) HeLa cells treated with TAMRA-modified single-strand DNA; (b) HeLa cells incubated with AuNPs modified with (**H**) and TAMRA-modified single-strand DNA (without the quencher); (c) HeLa cells incubated with AuNPs modified with (**H**) and fluorescence-quenched double-strand DNA (**1**). Scale bars are 20 μm.

solutions was measured under different conditions (Figure 2b). Curve a in Figure 2b shows that the fluorescence of (**1**) was effectively quenched. Without irradiation, no detectable fluorescence increment was observed in the presence of miRNA and EXO III (curve b). With irradiation, miRNA addition results in the significant fluorescence increment (curve c). The sample fluorescence increased with the increase of UV irradiation time, and the fluorescence intensity reached a plateau after 3 min irradiation (Figure S1). In our subsequent experiments, we used 3 min irradiation as the optimized UV irradiation time parameter. EXO III can indeed promote the DNA walker signal amplification, and the fluorescence intensity further increased with the addition of EXO III (curve d). With irradiation, the fluorescence intensity increased with the increase of EXO III concentration and the intensity reached a plateau when the concentration increased to 0.5 U/μL (Figure S2). In our subsequent experiments, we used 0.5 U/μL as the optimized EXO III concentration. With UV irradiation, the fluorescence intensity of the mixture solution increased with the increase of miRNA concentration, while no detectable fluorescence increment was observed without UV irradiation (Figure 2c). The fluorescence intensities of the mixture solutions treated with EXO III were much higher than the cases without EXO III treatment (Figure 2d). Polyacrylamide gel electrophoresis results showed that the (**F**) + (**Q**) line totally disappeared under the conditions of UV irradiation and EXO III treatment (Supporting Information, Figure S3). All these results proved that the light-activated DNA walker signal amplification assisted by EXO III was indeed proceeded, as shown in Figure 2a.

Photocontrollable DNA Walker System on the DNA Nanoflare Surface. Next, the photocontrollable DNA walker on the DNA nanoflare surface was demonstrated by immobilizing photoresponsive hairpin DNA (**H**) and double-strand DNA track (**1**) on the AuNP surface to fabricate the DNA nanoflares. Figure 3a shows the whole process. UV light was used to activate hairpin DNA (**H**) on the AuNP surface to initiate the displacement reaction with miRNA-21, releasing the DNA walker strand. The released DNA walker strand then hybridized with the fluorophore quencher-labeled DNA strand in surrounding DNA track (**1**), releasing the TAMRA-modified DNA strand (**2**) with turn-on fluorescence and forming double-strand DNA (**3**) with recessed 3′-termini. EXO III could then hydrolyze the fluorophore quencher-labeled DNA strand in newly formed double-strand DNA (**3**) from its 3′-termini to regenerate the DNA walker and trigger the DNA walker cascade recycling amplification process on the DNA nanoflare surface. The zeta potentials of AuNPs before and after DNA modification were −29.47 and −39.80 mV, respectively (Supporting Information, Figure S4c). The diameter of the AuNPs increased after (**1**) and (**H**) modification (Supporting Information, Figure S4d), which confirmed that the DNA was successfully modified on the AuNP surface. The UV irradiation-activated DNA walker on the DNA nanoflare surface was followed by measuring the DNA nanoflare fluorescence under different conditions. Curve a in Figure 3b shows that the fluorescence of the (**1**) probe immobilized on the AuNP surface was effectively quenched. Without UV irradiation, little fluorescence was detectable with the addition of miRNA and EXO III (Figure 3b, curve b). In turn, with UV irradiation and the addition of target miRNA-21, the TAMRA fluorescence of the system increased significantly (Figure 3b, curve c). The subsequent EXO III-assisted DNA walker signal amplification was proved by further fluorescence increment with EXO III addition (Figure 3b, curve d). With EXO III addition and UV irradiation, the fluorescence intensity increased with the increase of target concentrations from 0 to 100 pM and the fluorescence intensity achieved a platform at 200 pM (Figure 3c,d).

The specificity and photocontrollability of the DNA walker system were further demonstrated. As can be seen from Figure S5, in the cases of targets with one base insert, one base deletion, one base mismatch, and two bases' mismatch, the fluorescence intensity was significantly lower compared with

https://doi.org/10.1021/acs.analchem.1c04505
Anal. Chem. XXXX, XXX, XXX−XXX

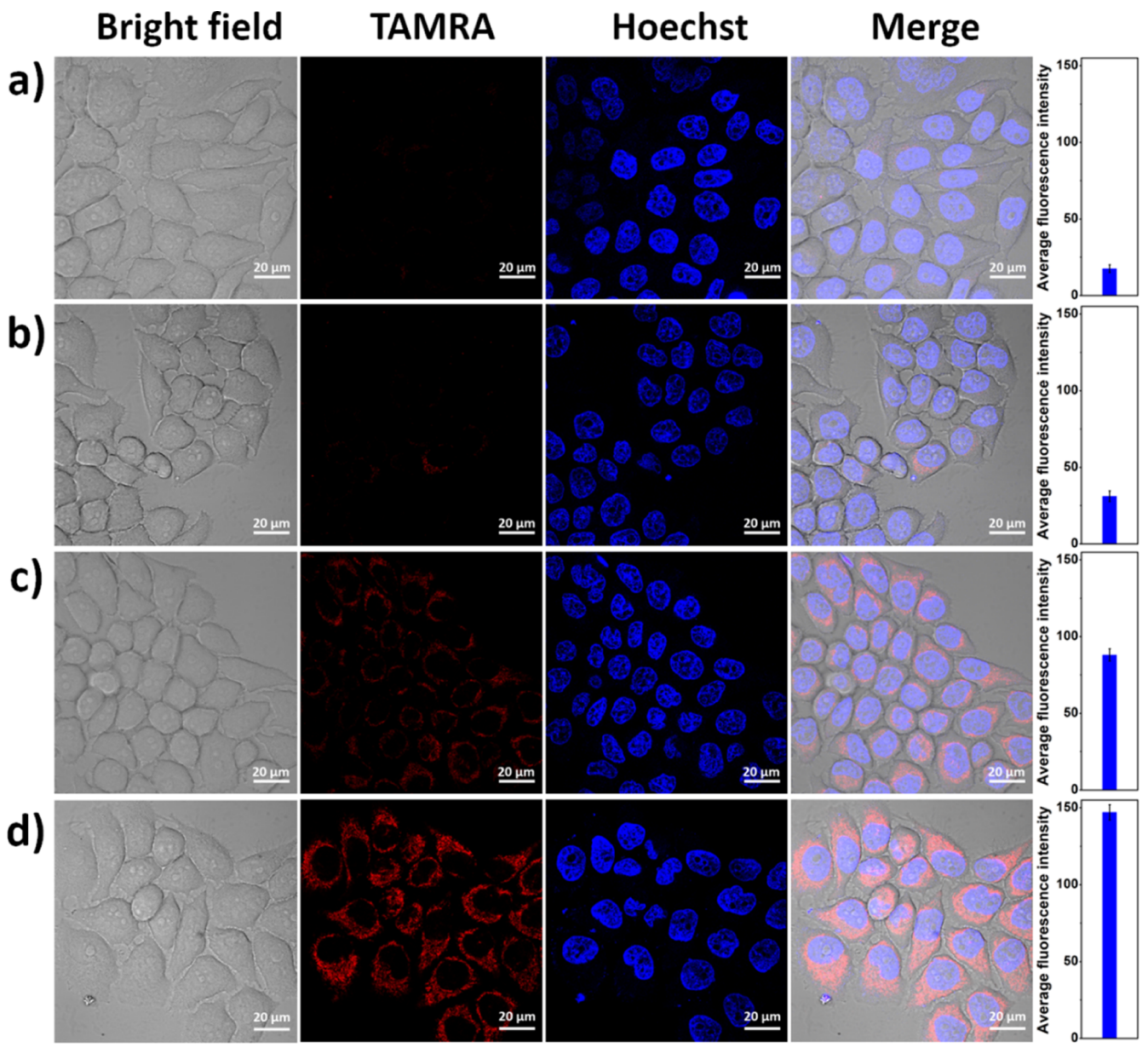

Figure 5. HeLa cell confocal microscopy imaging under different conditions. (a) HeLa cells treated with AuNPs modified with (**H**) and (**1**), without UV irradiation and EXO III treatment; (b) HeLa cells incubated with (**H**) and (**1**)-modified AuNPs and with EXO III treatment; (c) HeLa cells incubated with (**H**) and (**1**)-modified AuNPs and with UV irradiation; (d) HeLa cells incubated with (**H**) and (**1**)-modified AuNPs and with UV irradiation and EXO III treatment. Scale bars are 20 μm.

the case of perfectly matched target miRNA. This result demonstrated that our developed DNA walker system could effectively distinguish single base mutations. The photocontrollability and efficiency of the DNA walker system were tested by using DNA nanoflares without a PC-linker (normal hairpin structure), with a PC-linker (photoresponsive hairpin structure), and with the exposed toehold to perform the experiment (Supporting Information, Figure S6). The DNA nanoflare with a normal hairpin structure remained intact, and no fluorescence increase was observed even with 5 min UV irradiation (Supporting Information, Figure S6a). UV irradiation could activate the photoresponsive hairpin DNA (**H**) on DNA nanoflares and trigger the DNA walker system, resulting in the increase of the fluorescence with the increase of UV irradiation time (Supporting Information, Figure S6b). Figure S6c shows the fluorescence spectrum of the DNA walker system with the exposed toehold (the same situation as shown in Figure S6b after irradiation). The photoactivation efficiency was obtained by calculating the ratio of the fluorescence intensity at 585 nm in Figure S6b,c, and the calculated photoactivation efficiency is *ca.* 97% after 3 min UV irradiation.

Cell Endocytosis of DNA Nanoflares. After proving that our developed light-controllable DNA walker signal amplification system based on DNA nanoflares proceeded as designed, this DNA walker system was then used to achieve photoactivated signal amplification imaging of miRNA-21. As we need to follow the whole process in HeLa cells for miRNA imaging, the clear evidence for the internalization of photoresponsive functional DNA nanoflares into cells and the stability of the quenched fluorescence of the DNA nanoflares in the HeLa cells was essential. Thus, AuNPs decorated with photoresponsive DNA hairpin (**H**) and TAMRA-labeled

https://doi.org/10.1021/acs.analchem.1c04505
Anal. Chem. XXXX, XXX, XXX−XXX

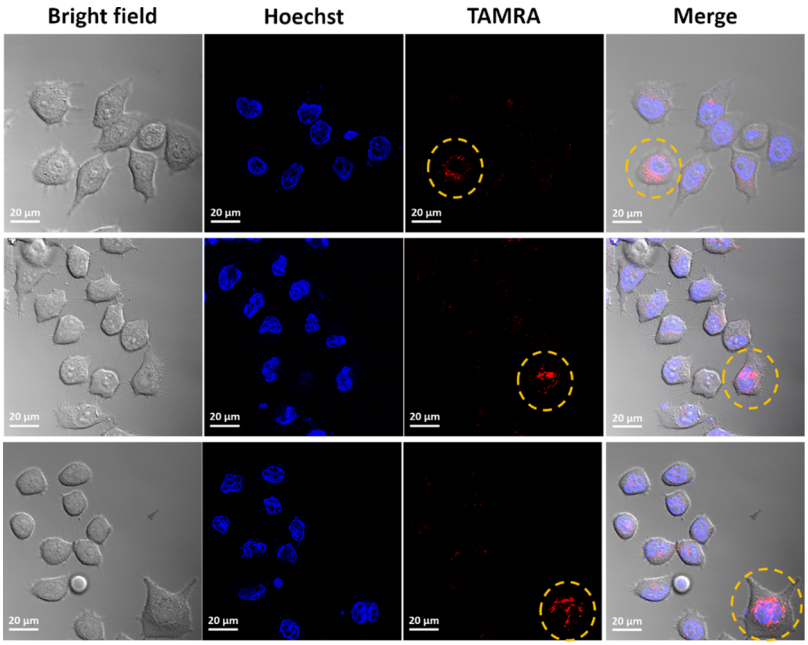

Figure 6. Spatial-controllable activation of DNA walker signal amplification in single living HeLa cells *via* two-photon irradiation. Circle-marked cells were spatial-controllably irradiated. The scale bars are 20 μm.

single-strand DNA or fluorescence-quenched double-strand track DNA (**1**) were used to demonstrate the internalization of DNA nanoflares and the stability of quenched fluorescence in HeLa cells. Cell fluorescence imaging in Figure 4a shows that the TAMRA-labeled single-strand DNA cannot go inside HeLa cells, whereas the TAMRA-labeled single-strand DNA immobilized on the AuNP surface could go inside into the cytoplasm assisted by the AuNPs (Figure 4b). Furthermore, no detectable fluorescence signal in HeLa cells was observed in the case of AuNPs modified with (**H**) and double-strand track DNA (**1**) with quenched fluorescence (Figure 4c), which means that the fluorescence quenching is effective and the DNA on the surface of internalized DNA nanoflares keeps intact in HeLa cells. The cell viability under different conditions was tested, and it shows that HeLa cells keep high vitality after incubating with DNA nanoflares, UV irradiation, and EXO III treatment (Supporting Information, Figure S7). The cells keep high viability after 10 min UV irradiation and long-time incubation (Supporting Information, Figure S8).

Photoactivated Signal-Amplified miRNA-21 Imaging in Living Cells. The light-triggered DNA walker signal amplification process in HeLa cells was followed by using a laser scanning confocal microscope. HeLa cells were incubated with AuNPs modified with (**H**) and (**1**). First, without UV irradiation, the AuNPs modified with (**H**) and (**1**) kept intact in HeLa cells and no detectable fluorescence signal was observed (Figure 5a). Without UV irradiation, the addition of EXO III could not result in significant fluorescence in HeLa cells, which means that EXO III could not promote DNA walker signal amplification without UV irradiation (Figure 3b). With UV irradiation, the (**H**) immobilized on the AuNP surface was photoactivated to initiate the displacement reaction with miRNA-21 in living HeLa cells, releasing the DNA walker strand. The released DNA walker then hybridized with the quencher-labeled DNA strand in surrounding (**1**), resulting in the slight fluorescence increment in living HeLa cells (Figure 5c). With UV irradiation, EXO III could promote the DNA walker signal amplification process. The fluorescence intensity in the case of EXO III-assisted DNA walker signal amplification is about 2-fold higher than the case without signal amplification in living HeLa cells (Figure 5d).

Two-Photon Irradiation-Activated Signal Amplification Imaging of miRNA-21 in Single Living HeLa Cells. Finally, to demonstrate the spatial controllability of our developed method, two-photon irradiation was used to spatially activate the photoresponsive (**H**) and trigger DNA walker signal amplification in irradiated single living HeLa cells. Laser scanning confocal microscopy with a femtosecond laser was used to selectively irradiate the single living HeLa cells. The irradiated cells were stained with 4 μM Calcein-AM (a commercial living cell probe) and 4 μM propidium iodide (PI, a commercial dead cell probe), and it shows that the cells keep high vitality (no PI signal was observed in irradiated cells) even after 60 min irradiation (Supporting Information, Figure S9). The photoresponsive (**H**) with a photocleavable *o*-nitrobenzylphosphate ester linker unit (PC-linker) could be activated *via* one-photon excitation (1PE, $\lambda \approx 365$ nm) or two-photon excitation (2PE, $\lambda = 740$).[40,43,47] Figure 6 shows that the signal amplification imaging of miRNA was spatial-controllably activated in circle-marked cells, resulting in the significant fluorescence increase in single living cells. No detectable fluorescence signal was observed in surrounding HeLa cells because the signal amplification cannot proceed in the cells without two-photon irradiation. These results demonstrated that the signal amplification strategy could achieve spatial-controllable activation in single living cells.

CONCLUSIONS

In conclusion, we introduce a signal amplification strategy termed as photoactivated DNA walker signal amplification based on DNA nanoflares, which enables spatiotemporally photocontrollable signal amplification miRNA imaging in single living cancer cells. The photoresponsive DNA hairpin-

https://doi.org/10.1021/acs.analchem.1c04505
Anal. Chem. XXXX, XXX, XXX−XXX

containing DNA walker was immobilized on the AuNP surface. Meanwhile, a double-strand DNA track with quenched fluorescence was also immobilized on the AuNP surface to fabricate the functional DNA nanoflares. The photoresponsive DNA hairpin on the AuNP surface was activated *via* one-photon irradiation (λ = 365 nm) or two-photon irradiation (λ = 740 nm) to trigger the nucleic acid displacement reaction in the presence of target miRNA-21, releasing the DNA walker strand. The released DNA walker could walk around the nearby fluorescence-quenched double-strand DNA track with the help of EXO III to light on the fluorescence. This photoactivated DNA walker system was further demonstrated in living cancer cells to achieve photocontrollable signal amplification imaging of miRNA-2 in HeLa cells. Furthermore, the developed method shows good temporal and spatial controllability and could control the time and position of the signal amplification in single living cancer cells on demand.

■ ASSOCIATED CONTENT

Supporting Information

The Supporting Information is available free of charge at https://pubs.acs.org/doi/10.1021/acs.analchem.1c04505.

Detailed nucleic acid sequences; UV irradiation time optimization; EXO III concentration optimization; native PAGE gel electrophoresis characterization; characterization of AuNPs and DNA nanoflares; specificity of the detection system; photocontrollability of the DNA walker; and cell viability of HeLa cells with different treatments (PDF)

■ AUTHOR INFORMATION

Corresponding Author

Fujian Huang − *State Key Laboratory of Biogeology and Environmental Geology, Engineering Research Center of Nano-Geomaterials of Ministry of Education, Faculty of Materials Science and Chemistry, China University of Geosciences, Wuhan 430074, China;* orcid.org/0000-0002-7777-1589; Email: huangfj@cug.edu.cn

Authors

Mengxi Chen − *State Key Laboratory of Biogeology and Environmental Geology, Engineering Research Center of Nano-Geomaterials of Ministry of Education, Faculty of Materials Science and Chemistry, China University of Geosciences, Wuhan 430074, China*

Ruilin Duan − *State Key Laboratory of Biogeology and Environmental Geology, Engineering Research Center of Nano-Geomaterials of Ministry of Education, Faculty of Materials Science and Chemistry, China University of Geosciences, Wuhan 430074, China*

Shijun Xu − *State Key Laboratory of Biogeology and Environmental Geology, Engineering Research Center of Nano-Geomaterials of Ministry of Education, Faculty of Materials Science and Chemistry, China University of Geosciences, Wuhan 430074, China*

Zhijuan Duan − *State Key Laboratory of Biogeology and Environmental Geology, Engineering Research Center of Nano-Geomaterials of Ministry of Education, Faculty of Materials Science and Chemistry, China University of Geosciences, Wuhan 430074, China*

Quan Yuan − *Institute of Chemical Biology and Nanomedicine, State Key Laboratory of Chemo/Biosensing and Chemometrics, College of Chemistry and Chemical Engineering, Hunan University, Changsha 410082, China;* orcid.org/0000-0002-3085-431X

Fan Xia − *State Key Laboratory of Biogeology and Environmental Geology, Engineering Research Center of Nano-Geomaterials of Ministry of Education, Faculty of Materials Science and Chemistry, China University of Geosciences, Wuhan 430074, China;* orcid.org/0000-0001-7705-4638

Complete contact information is available at: https://pubs.acs.org/10.1021/acs.analchem.1c04505

Notes

The authors declare no competing financial interest.

■ ACKNOWLEDGMENTS

This work was supported by the National Natural Science Foundation of China (21974127, 22090050, and 21874121), the National Key Research and Development Program of China (2018YFE0206900), the Hubei Provincial Natural Science Foundation of China (2020CFA037), and the Zhejiang Provincial Natural Science Foundation of China under grant nos. LD21B050001 and LY20B050001.

■ REFERENCES

(1) Dong, H.; Lei, J.; Ding, L.; Wen, Y.; Ju, H.; Zhang, X. *Chem. Rev.* **2013**, *113*, 6207−6233.

(2) Joglekar, M. V.; Wong, W. K. M.; Ema, F. K.; Georgiou, H. M.; Shub, A.; Hardikar, A. A.; Lappas, M. *Diabetologia* **2021**, *64*, 1516−1526.

(3) Zhuo, Z.; Wan, Y.; Guan, D.; Ni, S.; Wang, L.; Zhang, Z.; Liu, J.; Liang, C.; Yu, Y.; Lu, A.; Zhang, G.; Zhang, B. T. *Adv. Sci.* **2020**, *7*, 1903451.

(4) Cheng, J.; Meng, J.; Zhu, L.; Peng, Y. *Mol. Cancer* **2020**, *19*, 66.

(5) Esrick, E. B.; Lehmann, L. E.; Biffi, A.; Achebe, M.; Brendel, C.; Ciuculescu, M. F.; Daley, H.; MacKinnon, B.; Morris, E.; Federico, A.; Abriss, D.; Boardman, K.; Khelladi, R.; Shaw, K.; Negre, H.; Negre, O.; Nikiforow, S.; Ritz, J.; Pai, S.-Y.; London, W. B.; Dansereau, C.; Heeney, M. M.; Armant, M.; Manis, J. P.; Williams, D. A. *N. Engl. J. Med.* **2021**, *384*, 205−215.

(6) Hu, H.; Zhou, F.; Wang, B.; Chang, X.; Dai, T.; Tian, R.; Wan, Y.; Wang, X.; Wang, G. *Nanoscale* **2021**, *13*, 1863−1868.

(7) Luo, X.; Zhu, J.; Jia, W.; Fang, N.; Wu, P.; Cai, C.; Zhu, J.-j. *ACS Appl. Mater. Interfaces* **2021**, *13*, 18301−18313.

(8) Zhou, Y.; Yu, S.; Shang, J.; Chen, Y.; Wang, Q.; Liu, X.; Wang, F. *Anal. Chem.* **2020**, *92*, 15069−15078.

(9) Li, B.; Liu, Y.; Liu, Y.; Tian, T.; Yang, B.; Huang, X.; Liu, J.; Liu, B. *ACS Nano* **2020**, *14*, 8116−8125.

(10) Miao, P.; Tang, Y. *Anal. Chem.* **2020**, *92*, 12026−12032.

(11) Bodulev, O. L.; Zhao, S.; Sakharov, I. Y. *Anal. Chem.* **2021**, *93*, 6824−6830.

(12) Zhang, P.; Ouyang, Y.; Sohn, Y. S.; Nechushtai, R.; Pikarsky, E.; Fan, C.; Willner, I. *ACS Nano* **2021**, *15*, 6645−6657.

(13) Duan, R.; Zuo, X.; Wang, S.; Quan, X.; Chen, D.; Chen, Z.; Jiang, L.; Fan, C.; Xia, F. *Nat. Protoc.* **2014**, *9*, 597−607.

(14) Qu, X.; Zhu, D.; Yao, G.; Su, S.; Chao, J.; Liu, H.; Zuo, X.; Wang, L.; Shi, J.; Wang, L.; Huang, W.; Pei, H.; Fan, C. *Angew. Chem., Int. Ed.* **2017**, *56*, 1855−1858.

(15) Liu, Z.; Lei, S.; Zou, L.; Li, G.; Ye, B. *Biosens. Bioelectron.* **2020**, *167*, 112487.

(16) Cai, R.; Zhang, S.; Chen, L.; Li, M.; Zhang, Y.; Zhou, N. *ACS Appl. Mater. Interfaces* **2021**, *13*, 4905−4914.

(17) Huang, X.-B.; Wu, S.-H.; Hu, H.-C.; Sun, J.-J. *ACS Sens.* **2020**, *5*, 2636−2643.

(18) Liu, S.; Yu, X.; Wang, J.; Liu, D.; Wang, L.; Liu, S. *Anal. Chem.* **2020**, *92*, 9764−9771.

(19) Duan, R.; Li, T.; Duan, Z.; Huang, F.; Xia, F. *Anal. Chem.* **2020**, *92*, 5846−5854.
(20) Memon, A. G.; Xing, Y.; Zhou, X.; Wang, R.; Liu, L.; Zeng, S.; He, M.; Ma, M. *J. Hazard. Mater.* **2020**, *384*, 120948.
(21) Wang, Z.-G.; Elbaz, J.; Willner, I. *Nano Lett.* **2011**, *11*, 304−309.
(22) Xue, Y.; Wang, Y.; Feng, S.; Yan, M.; Huang, J.; Yang, X. *Anal. Chem.* **2021**, *93*, 8962−8970.
(23) Chao, J.; Wang, J.; Wang, F.; Ouyang, X.; Kopperger, E.; Liu, H.; Li, Q.; Shi, J.; Wang, L.; Hu, J.; Wang, L.; Huang, W.; Simmel, F. C.; Fan, C. *Nat. Mater.* **2019**, *18*, 273−279.
(24) Kwon, P. S.; Ren, S.; Kwon, S.-J.; Kizer, M. E.; Kuo, L.; Xie, M.; Zhu, D.; Zhou, F.; Zhang, F.; Kim, D.; Fraser, K.; Kramer, L. D.; Seeman, N. C.; Dordick, J. S.; Linhardt, R. J.; Chao, J.; Wang, X. *Nat. Chem.* **2020**, *12*, 26−35.
(25) Ebrahimi, S. B.; Samanta, D.; Mirkin, C. A. *J. Am. Chem. Soc.* **2020**, *142*, 11343−11356.
(26) Seferos, D. S.; Giljohann, D. A.; Hill, H. D.; Prigodich, A. E.; Mirkin, C. A. *J. Am. Chem. Soc.* **2007**, *129*, 15477−15479.
(27) Samanta, D.; Ebrahimi, S. B.; Mirkin, C. A. *Adv. Mater.* **2020**, *32*, 1901743.
(28) Li, J.; Wang, J.; Liu, S.; Xie, N.; Quan, K.; Yang, Y.; Yang, X.; Huang, J.; Wang, K. *Angew. Chem., Int. Ed.* **2020**, *59*, 20104−20111.
(29) Li, J.; Cai, S.; Zhou, B.; Meng, X.; Guo, Q.; Yang, X.; Huang, J.; Wang, K. *Chem. Commun.* **2020**, *56*, 6126−6129.
(30) Liang, C.-P.; Ma, P.-Q.; Liu, H.; Guo, X.; Yin, B.-C.; Ye, B.-C. *Angew. Chem., Int. Ed.* **2017**, *56*, 9077−9081.
(31) Cui, M.-R.; Xiangling, L.; Chen, H.-Y.; Xu, J.-J. *CCS Chem.* **2020**, *3*, 2063−2073.
(32) Pang, H.; Xu, X.; Jiang, W. *Sens. Actuators, B* **2020**, *314*, 128053.
(33) Yang, X.; Tang, Y.; Mason, S. D.; Chen, J.; Li, F. *ACS Nano* **2016**, *10*, 2324−2330.
(34) Wang, C.; Han, Q.; Mo, F.; Chen, M.; Xiong, Z.; Fu, Y. *Anal. Chem.* **2020**, *92*, 12145−12151.
(35) Qing, Z.; Xu, J.; Hu, J.; Zheng, J.; He, L.; Zou, Z.; Yang, S.; Tan, W.; Yang, R. *Angew. Chem., Int. Ed.* **2019**, *58*, 11574−11585.
(36) Peng, H.; Newbigging, A. M.; Reid, M. S.; Uppal, J. S.; Xu, J.; Zhang, H.; Le, X. C. *Anal. Chem.* **2020**, *92*, 292−308.
(37) Yang, Y.; Huang, J.; Yang, X.; He, X.; Quan, K.; Xie, N.; Ou, M.; Wang, K. *Anal. Chem.* **2017**, *89*, 5850−5856.
(38) Sengupta, D.; Deb, M.; Kar, S.; Pradhan, N.; Parbin, S.; Kirtana, R.; Singh, S. P.; Suma, S. G.; Niharika; Roy, A.; Manna, S.; Saha, P.; Chakraborty, P.; Dash, S.; Kausar, C.; Patra, S. K. *Semin. Cancer Biol.* **2021**, *72*, 46−64.
(39) Huang, F.; You, M.; Han, D.; Xiong, X.; Liang, H.; Tan, W. *J. Am. Chem. Soc.* **2013**, *135*, 7967−7973.
(40) Huang, F.; Chen, M.; Zhou, Z.; Duan, R.; Xia, F.; Willner, I. *Nat. Commun.* **2021**, *12*, 2364.
(41) Huang, F.; Xu, H.; Tan, W.; Liang, H. *ACS Nano* **2014**, *8*, 6849−6855.
(42) Huang, F.; Zhou, X.; Yao, D.; Xiao, S.; Liang, H. *Small* **2015**, *11*, 5800−5806.
(43) Huang, F.; Zhang, J.; Li, T.; Duan, R.; Xia, F.; Willner, I. *Nano Lett.* **2019**, *19*, 618−625.
(44) Lin, M.; Yi, X.; Wan, H.; Zhang, J.; Huang, F.; Xia, F. *Anal. Chem.* **2020**, *92*, 9963−9970.
(45) Huang, F.; Liao, W.-C.; Sohn, Y. S.; Nechushtai, R.; Lu, C.-H.; Willner, I. *J. Am. Chem. Soc.* **2016**, *138*, 8936−8945.
(46) Huang, F.; Duan, R.; Zhou, Z.; Vázquez-González, M.; Xia, F.; Willner, I. *Chem. Sci.* **2020**, *11*, 5592−5600.
(47) Lin, M.; Yi, X.; Huang, F.; Ma, X.; Zuo, X.; Xia, F. *Anal. Chem.* **2019**, *91*, 2021−2027.
(48) Huang, F.; Lin, M.; Duan, R.; Lou, X.; Xia, F.; Willner, I. *Nano Lett.* **2018**, *18*, 5116−5123.

https://doi.org/10.1021/acs.analchem.1c04505
Anal. Chem. XXXX, XXX, XXX−XXX